Tunable Class E^2 DC–DC Converter With High Efficiency and Stable Output Power for 6.78-MHz Wireless Power Transfer

Shuangke Liu, *Student Member, IEEE*, Ming Liu, *Member, IEEE*, Songyang Han, *Student Member, IEEE*, Xinen Zhu, *Member, IEEE*, and Chengbin Ma, *Member, IEEE*

***Abstract*—Class E^2 DC–DC converter composed of Class E power amplifier (PA) and rectifier is a promising candidate for MHz wireless power transfer. It is soft-switching based and able to achieve high efficiency at MHz frequency. However, the converter implemented through traditional static design is sensitive to the variations of operation condition. Its performance gets deteriorated when DC load and coil coupling deviate from their respective optimum values. This paper demonstrates that the degradation of system efficiency is mostly due to the mismatch of PA load, and the efficiency drop can be efficiently improved by adding an L-type impedance matching network (IMN) after PA. A fixed IMN is sufficient to maintain a high efficiency, while a tunable IMN is required to ensure stable output power when operation condition dramatically changes. Key techniques, particularly system-level optimization, are discussed in this paper that ensure high efficiency over a wide range of variation in operation condition and also with reduced capacitor/inductor tuning ranges in the IMN. The 6.78-MHz Class E^2 DC–DC converters with and without the fixed/tunable IMN are fabricated and measured for validation purposes. The experimental results show that both high efficiency (>66%) and stable output power (around 9 W) are maintained for the tunable converter when there are variations in the DC load and coil coupling.**

***Index Terms*—High efficiency, megahertz wireless power transfer (WPT), stable output power, tunable Class E^2 DC–DC converter, tunable impedance matching network (IMN).**

I. Introduction

WIRELESS power transfer (WPT) systems working at MHz have been receiving increasing research attention in recent years due to their advantages of larger spatial freedom and compact circuit size [1], [2]. However, the switching loss occurred in MOSFET and diode could also become considerably large at high frequencies. The traditional hard-switching-based inverters and rectifiers, such as the full-bridge inverter and rectifier used in kHz WPT systems, are usually not suitable for being directly applied in the MHz systems. Class E^2 DC–DC converter, composed of soft-switching-based Class E power amplifier (PA) and Class E rectifier, is a promising solution for a high-efficiency operation in MHz WPT applications.

The Class E PA was first proposed in 1975 [3]. It has been widely used thanks for its simple topology and high efficiency [4], [5]. The drain voltage of an ideal Class E PA reaches zero prior to turn on of the MOSFET, which theoretically results in zero switching loss. High efficiency of the Class E PA up to 94% at MHz frequency has been observed in experiments [4]. The Class E rectifier applied in WPT systems was initially presented in [6], in which an efficiency of 94% at 800 kHz was achieved. In the rectifier, a capacitor is connected in parallel with the diode such that the diode turns ON and OFF with low dv_D/dt (v_D is the voltage across the diode), namely reduced switching loss. Due to the soft-switching property of the Class E PA and rectifier, the Class E^2 DC–DC converter is able to achieve high efficiency in MHz WPT applications [7]–[9]. Traditional design of Class E^2 DC–DC converter is a static one. The DC load and coupling coefficient are assumed to be constant. The circuit parameters are then designed to let each subsystem of the DC–DC converter (i.e., PA, coupling coils, and rectifier) operate under optimum conditions [8], [9]. However, in real applications, a WPT system may work under a changing operation condition. The coupling coefficient may change due to the coil misalignment. The load of rectifier could also vary over time such as when charging a battery. Beh *et al.* [10] show that the system efficiency ranges from 15% to 90% when the ratio of transfer distance to coil diameter changes from 0.2 to 1.4. The system efficiency drop caused by the coil misalignment is due to both the deteriorated coil performance and the load mismatch of power source [11]. In [12], a robust Class E^2 WPT system is designed, in which the coupling coefficient and DC load change from 0.1 to 0.4 and 15 to 45 Ω, respectively. The system efficiency itself is improved significantly when the coil coupling and DC load vary. However, at the same time, the output power varies dramatically from about 2.5 to 18 W. The existing design of the Class E^2 WPT system still cannot fully adapt to the varying operation conditions, particularly its incapability of maintaining stable output power.

Manuscript received January 4, 2017; revised June 11, 2017; accepted September 26, 2017. Date of publication October 12, 2017; date of current version April 20, 2018. This work was supported by the Shanghai Natural Science Foundation under Grant 16ZR1416300. Recommended for publication by Associate Editor M. Duffy. *(Corresponding author: Chengbin Ma.)*

S. Liu, S. Han, and C. Ma are with the University of Michigan–Shanghai Jiao Tong University Joint Institute, Shanghai Jiao Tong University, Shanghai 200240, China (e-mail: liushuangke@sjtu.edu.cn; hansongyang@sjtu.edu.cn; chbma@sjtu.edu.cn).

M. Liu is with the Department of Electrical Engineering, Princeton University, Princeton, NJ 08544 USA (e-mail: ml45@princeton.edu).

X. Zhu is with the Shanghai Industrial μTechnology Research Institute, Shanghai 201800, China (e-mail: alfred.zhu@sitrigroup.com).

Color versions of one or more of the figures in this paper are available online at http://ieeexplore.ieee.org.

Digital Object Identifier 10.1109/TPEL.2017.2762924

Many solutions have been proposed to improve system efficiency through subsystem-level optimization and optimum load tracking. In [13]–[16], the duty cycle of driving signal, operation frequency, and inductor are tuned to make the Class E PA operate under optimum switching conditions when the coil misalignment occurs. The degradation of coil performance caused by the misalignment can be mitigated via adaptive frequency matching, tuning of compensation capacitors, field shaping, and coupling adjustment using multi-coil system as given in [17]–[23]. These tuning and control techniques used for subsystem-level optimization cannot ensure a high efficiency of the overall WPT system and particularly the stable output power. In addition, the tuning ranges of the control variables may become considerably large with dramatically varied operation condition. Multiple control methods could be combined together to achieve significant improvement. However, this inevitably increases the complexity in real implementation. In [24]–[26], the system efficiency is improved by optimum load tracking. An additional DC–DC converter is added after the rectifier. The duty cycles of their switches are adaptively controlled to provide an optimum load to the overall WPT system. But in this solution, the output DC voltage may vary violently, which is usually undesirable in real applications. Santiago-González *et al.* [27] and Roslaniec *et al.* [28] focus on the parameter design for robust Class E PA and rectifier, respectively, under a varying operating condition. Generally, it is important to perform a comprehensive system-level analysis of the Class E^2 WPT system. The analysis helps to locate a specific subsystem that is the most sensitive to the variations in coupling coefficient and DC load. Thus, an effective and practical solution can be proposed and discussed later.

This paper is organized as follows. Section II discusses the Class E^2 DC–DC converter based on the traditional static design. The analysis shows that the system efficiency drop is mainly caused by the mismatch of PA load to its optimum value. Then, Section III explains that high-performance Class E^2 DC–DC converter under varying operation conditions can be achieved by adding an L-type impedance matching network (IMN) between the PA and coupling coils. A single fixed IMN is sufficient to maintain the high efficiency of the WPT system. Meanwhile, a tunable IMN has to be applied for providing stable output power. Techniques that reduce the tuning ranges of the tunable components are developed based on system-level analysis and optimization. Different with traditional impedance matching in RF/microwave circuits, the PA loads are transformed to a targeted region in the Smith chart instead of one single value (usually the conjugate source impedance). The tuning ranges of the tunable capacitor and inductor were narrowed down 29% and 46%, respectively, through properly adjusting the PA and coupling coils. Thus, the real implementation of the tunable IMN circuit is largely simplified. Finally, the Class E^2 DC–DC converters for 6.78 MHz WPT with and without fixed/tunable IMNs are fabricated and tested in experiments in Section IV. The results show that the tunable converter and the converter with fixed IMN are able to maintain a high efficiency over 66% when the DC load and coupling coefficient vary from 10 to 100 Ω and 0.1 to 0.4, respectively; while the efficiency of the conventional converter is 20% in the worst case. The output power of the tunable converter maintains around 9 W. On the other hand, the output power changes dramatically from 2 to 15.2 W in the conventional converter and 0.96 to 20.4 W in the converter with fixed IMN.

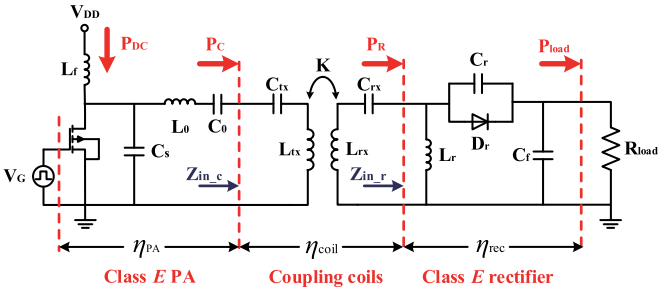

Fig. 1. Configuration of a typical Class E^2 DC–DC converter for WPT applications.

TABLE I
PARAMETERS OF THE CLASS E^2 DC–DC CONVERTER

PA	L_f (10 μ H)	RF choke
	C_s (215 pF)	shunt capacitor
	L_0 (1.42 μ H)	filter inductor
	C_0 (626 pF)	filter capacitor
Coils	L_{tx} (3.24 μ H)	inductance of transmitting coil
	r_{tx} (0.7 Ω)	equivalent series resistance of L_{tx}
	C_{tx} (165 pF)	compensation capacitor of L_{tx}
	L_{rx} (3.24 μ H)	inductance of receiving coil
	r_{rx} (0.7 Ω)	equivalent series resistance of L_{rx}
	C_{rx} (195 pF)	compensation capacitor of L_{rx}
	k (0.1 to 0.4)	coupling coefficient
Rectifier	L_r (68 μ H)	RF choke
	r_{L_r} (0.2 Ω)	equivalent series resistance of L_r
	C_r (200 pF)	shunt capacitor of diode
	r_{D_r} (1.4 Ω)	on-resistance of diode
	C_f (44 μ F)	DC filter capacitor

II. ANALYSIS OF CONVENTIONAL CLASS E^2 DC–DC CONVERTER

Fig. 1 shows a typical configuration of a Class E^2 DC–DC converter used in WPT applications. It consists of a Class E PA, coupling coils, and a Class E rectifier. The parameters of the WPT system are listed in Table I. $Z_{\text{in\_}r}$ and $Z_{\text{in\_}c}$ are the equivalent loads of the coupling coils and PA, respectively. P_{DC}, P_C, P_R, and P_{load} are the input DC power, input power of coupling coils, input power of rectifier, and output DC power, respectively. The subsystem-level efficiencies, η_{PA}, η_{coil}, and η_{rec}, are defined in (1), and the system efficiency is the product of these three efficiencies, as shown in (2)

$$\eta_{PA} = \frac{P_C}{P_{\text{DC}}}, \quad \eta_{\text{coil}} = \frac{P_R}{P_C}, \quad \eta_{\text{rec}} = \frac{P_{\text{load}}}{P_R} \tag{1}$$

$$\eta_{\text{sys}} = \eta_{PA} \cdot \eta_{\text{coil}} \cdot \eta_{\text{rec}}. \tag{2}$$

The influence on the overall system performance caused by the variations in the coupling coefficient k and DC load R_{load} is investigated as follows. Simulation models are built with an operating frequency of 6.78 MHz using Advance Design System from Keysight Technologies. The Spice models of SUD06N10

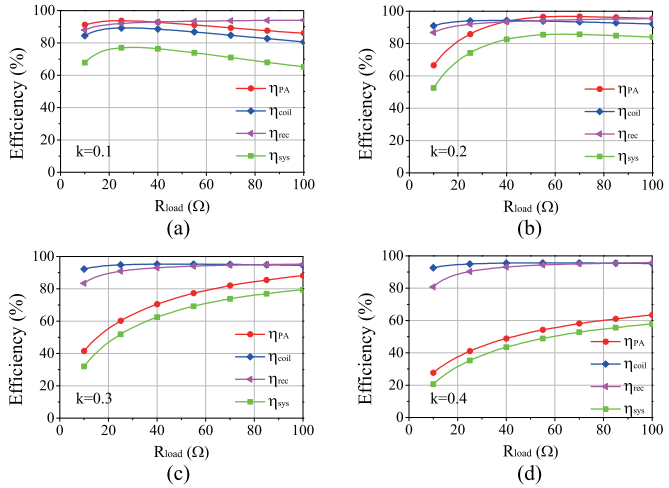

Fig. 2. Efficiencies of overall system, Class E PA, coupling coils, and Class E rectifier with varying k (0.1–0.4) and R_{load} (10–100 Ω). (a) $k = 0.1$. (b) $k = 0.2$. (c) $k = 0.3$. (d) $k = 0.4$.

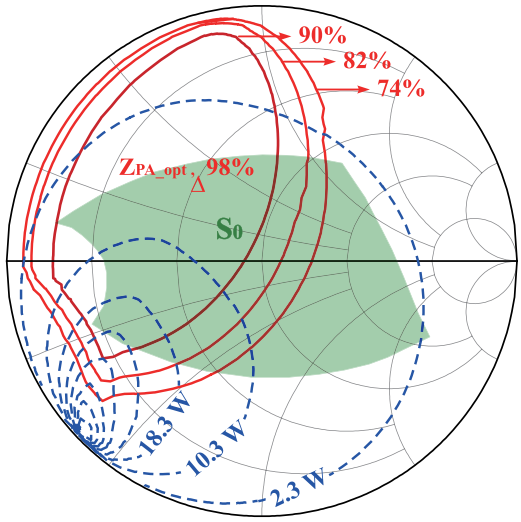

Fig. 3. Load-pull simulation results of the Class E PA and $Z_{\text{in\_}c}$ with varying k (0.1–0.4) and R_{load} (10–100 Ω).

(MOSFET) and STPSC406D (Diode) provided by manufacturers are adopted in the simulation. Here, the DC supply voltage is kept constant, 20 V. Liu *et al.* [9] developed static design procedures for a WPT system employing the same configuration in Fig. 1. Basically, the rectifier is first designed to enable a 50% duty cycle of the rectifying diode. With the analytically derived input impedance of the rectifier, the compensation capacitor of the receiving coil is optimally determined that makes the two coupling coils exactly resonant. Finally, the PA is designed to achieve zero-voltage-switching (ZVS) condition and thus maximize its efficiency targeting on the derived load seen by the PA (i.e., the input impedance of the coupling coils).

The Class E^2 DC–DC converter under an optimum operation condition can achieve a maximum efficiency of 84% in the above simulation. However, its performance may quickly deteriorate due to variations in k and R_{load}. Fig. 2(a)–(d) shows the efficiencies of the overall system, coupling coils, Class E rectifier, and Class E PA when k and R_{load} vary. The results explain that the Class E PA is the most sensitive to the varying k and R_{load}.

Fig. 3 gives the load-pull simulation results of the Class E PA. Two groups of contours are shown in the Smith chart, the constant power and constant efficiency contours. Note that the Smith charts are normalized to 50 Ω [29]. The equivalent loads of PA with varying k (0.1–0.4) and R_{load} (10–100 Ω) are also depicted in the Smith chart, as illustrated by the green region S_0 in Fig. 3. Only a small part of S_0 is close to the location of the optimum load $Z_{\text{PA\_opt}}$ (the red triangle). This explains the low PA efficiency when k and R_{load} deviate from their respective optimum values. Contours with different constant power also pass S_0 indicating a wide range of variation in the PA output power. The above simulation results and analysis show that the deterioration of the system performance is mostly due to the mismatch of the PA load. It is expected that the performance of the Class E^2 DC–DC converter (i.e., both high efficiency and stable output power) can be significantly improved by matching the PA load to its preferred values. In the following section, impedance matching is analyzed and performed through designing a tunable IMN, which is located between the PA and coupling coils. This tunable IMN works to improve the operation condition of the PA without degrading the performance of the coupling coils and rectifier.

III. Design of Tunable Converter

The above deteriorated performance (i.e., low efficiency and instable output power) of the Class E^2 DC–DC converter can be improved by adding an L-type IMN between the PA and coupling coils. From Fig. 3, it can be seen that, in addition to the optimum load $Z_{\text{PA\_opt}}$, high efficiency can also be achieved if $Z_{\text{in\_}c}$ locates within the high-efficiency region in the Smith chart. Here, the region inside the 90% efficiency contour is taken as a high-efficiency region. A fixed IMN is sufficient to maintain a high system efficiency by ensuring that all $Z_{\text{in\_}c}$'s stay within the high-efficiency region. Section III-A discusses the influence of the IMN on the system performance and presents design procedures that enable high efficiency over a wide range of variations in operation condition. The advantage of the fixed IMN is its simple circuit and easy implementation. Meanwhile, the output power may still vary substantially when there are large variations in the operation condition. In such cases, a tunable IMN is necessary to transform all $Z_{\text{in\_}c}$'s to a much more narrow region, which corresponds to both high efficiency and preferred power level, namely the overlap between the high efficiency region and the nearby area of a specific power contour. However, the required tuning ranges of inductor and capacitor may become very large if the IMN is directly applied without system-level optimization. As explained in Section III-B, through properly adjusting the PA and coupling coils, the tuning ranges of the components can be significantly reduced. This makes the designed tunable IMN more practical and easier to be implemented.

A. Converter With the Fixed IMN

The IMN has been extensively used in communication systems to achieve maximum output power [30]–[32]. The most

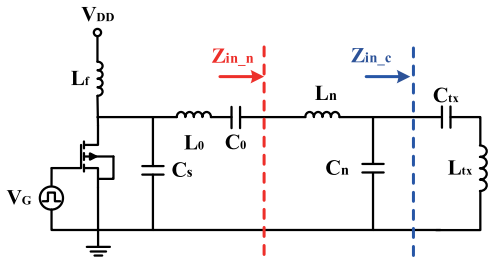

Fig. 4. Fixed IMN added between the PA and coupling coils.

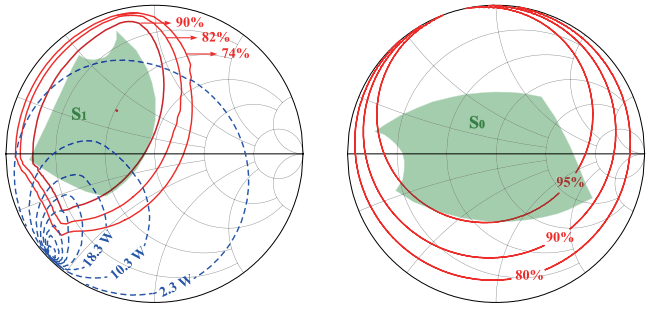

Fig. 5. Input impedance of the fixed IMN ($Z_{\text{in\_}n}$) and efficiency distribution of the L-type IMN. (a) $Z_{\text{in\_}n}$ with varying R_{load} (10–100 Ω) and k (0.1–0.4). (b) Efficiency contours of the L-type IMN.

frequently used IMNs are the L-, Pi-, and T-type networks. The Pi- and T-type IMNs compose of three components and thus are theoretically capable to match any impedance. They provide a higher degree of design freedom to perform not only impedance matching but also other functions such as harmonic rejection. However, the Pi- and T-type IMNs are difficult to control because there is infinite number of possible combinations available for a specific impedance matching problem. Besides, the Pi-/T-type IMN itself may introduce lots of power loss. The L-type IMN consists of only two components, namely potential for high-efficiency operation. Its solution, namely, the values of the inductor and capacitor, is also unique for a certain load. A disadvantage of the L-type IMN is that its capability of impedance matching is limited [33]. In WPT applications, efficiency is usually with a high priority. Thus, in this paper the L-type IMN is applied to transform PA load to preferred values. The PA, coupling coils, and rectifiers should be carefully designed such that one single L-type IMN is capable to match all the preferred impedances when the operation condition changes.

The L-type IMN is added between the PA and coupling coils, as shown in Fig. 4. The design target of the fixed L-type IMN is to transform all $Z_{\text{in\_}c}$'s to the high-efficiency region in the Smith chart and also as close as possible to $Z_{\text{PA\_opt}}$. Analytic expressions of input impedance of the rectifier, coupling coil, and IMN are expressed in the following equations:

$$Z_{\text{in\_}r} = R_{\text{rec}} + jX_{\text{rec}} \tag{3}$$

where

$$\begin{cases} R_{\text{rec}} = 0.5768(R_{\text{load}} + r_{L_r}) + 0.7116 r_{D_r} \\ X_{\text{rec}} = -[0.6648(R_{\text{load}} + r_{L_r}) + 0.8484 r_{D_r}] \end{cases}$$

$$Z_{\text{in\_}c} = \frac{\omega^2 k^2 L_t L_r}{r_{rx} + R_{\text{rec}} + jX_{\text{rec}}} + r_{tx} \tag{4}$$

$$Z_{\text{in\_}n} = j\omega L_n + \frac{Z_{\text{in\_}c}}{j\omega C_n Z_{\text{in\_}c} + 1}. \tag{5}$$

It can be seen that $Z_{\text{in\_}n}$ is a function of R_{load}, k, L_n, and C_n. A numerical optimization method such as genetic algorithm can be applied to find the optimum L_n and C_n that minimize (6) when R_{load} and k vary in a specific range. Note that $\Gamma_{\text{in\_}n}$ and $\Gamma_{\text{PA\_opt}}$ are the reflection coefficients corresponding to $Z_{\text{in\_}n}$ and $Z_{\text{PA\_opt}}$, respectively

$$\sum_{\text{k}} \sum_{\text{R}_{\text{load}}} | \Gamma_{\text{in\_}n} - \Gamma_{\text{PA\_opt}} | \tag{6}$$

where

$$\Gamma_{\text{in\_}n} = \frac{Z_{\text{in\_}n} - 50}{Z_{\text{in\_}n} + 50}, \quad \Gamma_{\text{PA\_opt}} = \frac{Z_{\text{PA\_opt}} - 50}{Z_{\text{PA\_opt}} + 50}.$$

Here, $L_n = 690$ nH and $C_n = 600$ pF are calculated to obtain the minimum (6) when R_{load} and k change from 10 to 100 Ω and 0.1 to 0.4, respectively. Fig. 5 illustrates the distribution of $Z_{\text{in\_}n}$, which is presented by the green region S_1 in the Smith chart. Almost all $Z_{\text{in\_}n}$'s are within the constant efficiency contour of 90%. This indicates that the PA efficiency maintains high even when R_{load} and k vary in a wide range. Adding the IMN also introduces extra power consumption due to the equivalent series resistances (ESRs) of the inductor and capacitor. However, the power consumption of IMN is much less than the switching loss caused by the PA load mismatch. Fig. 5(b) shows the efficiency distribution of the IMN in the Smith chart when the Q factor of L_n is 80. The IMN keeps operating in a high efficiency above 95% under most operation conditions.

The fixed IMN ensures a high efficiency of the WPT system, but with dramatically varying output power. As shown in Fig. 5(a), the PA output power ranges from 0.8 to 22.6 W when the fixed IMN is applied. This large variation range of output power is usually unfavorable in real applications. It is theoretically possible to have a controllable DC power supply that confines the output power to a preferred range. However, this may require a very high DC supply voltage that leads to a high drain voltage and thus the possible damage of the MOSFET. Adding an additional L-type IMN after PA cannot further shrink the area of S_1, and the ESRs of the added inductors and capacitors increase the power consumption of IMN. Thus, the Class E PA with the fixed L-type IMN is suitable for the applications with limited variation in the operation condition. A tunable IMN becomes necessary when the operation condition changes in a wide range and stable output power is required at the same time.

B. *Tunable Converter With Reduced Tuning Range*

The tunable IMN shares the same basic configuration with the fixed IMN. But its inductor L_{n_t} and capacitor C_{n_t} are tunable. As shown in Fig. 6, a target region T_1, which is within the 90% efficiency contour and close to the constant 10-W power contour, is specified in the Smith chart. Thus, high efficiency

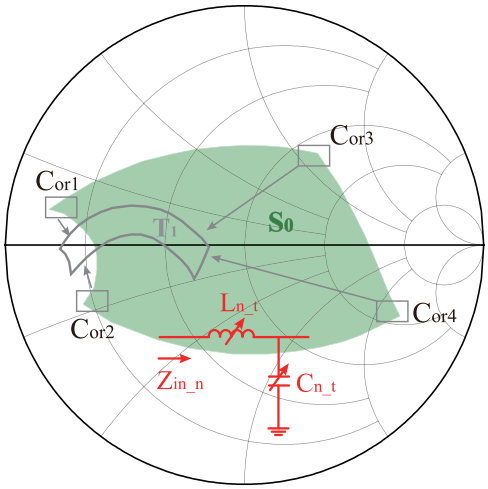

Fig. 6. Tunable IMN and target region T_1.

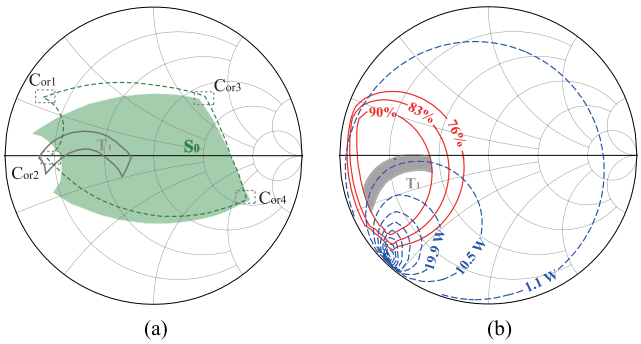

Fig. 7. Reposition of input impedance $Z_{\text{in\_}c}$ and target region T_1. (a) $Z_{\text{in\_}c}$ when C_{tx} changes to 175 pF. (b) Target region T_1 when C_s in PA is adjusted to 420 pF.

and stable output power can be simultaneously achieved by transforming all $Z_{\text{in\_}c}$'s to T_1 through the tunable IMN. The maximum and minimum values of L_{n_t} and C_{n_t} are obtained by calculating the inductances and capacitances required for the load transform, namely from the four corners of S_0, (i.e., C_{or1}–C_{or4}) to T_1. Here, $C_{\min}$, $C_{\max}$, $L_{\min}$, and $L_{\max}$ that achieve the above load transform are 0 pF, 2400 pF, 0 nH, and 1400 nH, respectively.

As shown above, the tuning ranges of L_{n_t} and C_{n_t} are large when the tunable IMN is directly applied without further optimization. These large ranges make it challenging to implement the IMN circuit. Many tuning states have to be included to ensure the effectiveness of the tunable IMN. It is practically important to reduce the tuning ranges of L_{n_t} and C_{n_t}.

The value of $C_{\max}$ is due to C_{or1}. It can be reduced by enlarging the capacitor C_{tx} connected in series with the transmitting coil. Note that adjusting C_{tx} does not impact the coil efficiency. In Fig. 7(a), the new region of $Z_{\text{in\_}c}$ is outlined by the dash line when a larger C_{tx} is applied. Continuously increasing C_{tx} can further reduce $C_{\max}$. But it requires a larger $L_{\max}$. Here, $C_{\max}$ is reduced from the original 2400 pF to 1700 pF by enlarging C_{tx} to 175 pF.

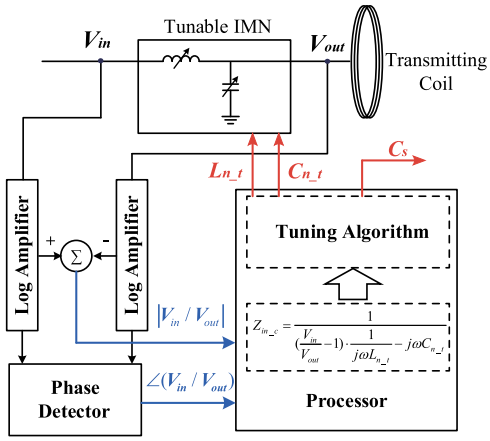

Fig. 8. Block diagram of a dynamic IMN tuning system.

$L_{\max}$ is determined by C_{or4}. A smaller $L_{\max}$ can be achieved by modifying the parameters of the PA. In real applications, large inductors are usually undesirable not only because of the increased number of tuning states but also due to the fact that inductor is an actual device that consumes power and space. The quality factor of inductors is usually much lower than that of capacitors. Considerable power could be consumed by the IMN if a large inductor is applied. In this paper, $L_{\max}$ is reduced through repositioning T_1. It is found that the inductor required to transform C_{or4} into T_1 is reduced by moving T_1 to the lower part of the Smith chart [see Fig. 7(b)]. The reposition of T_1 is realized with the cost of having a tunable component in the PA, the shunt capacitor C_s. But this makes it possible to effectively redistribute the constant efficiency and power contours of PA. Fig. 7(b) shows the load-pull simulation results of the Class E PA with an adjusted C_s (420 pF). The position of the high-efficiency region becomes lower comparing with that of the case when the PA is with original C_s (215 pF). In the following experiments, C_s is switched from 215 pF to 420 pF when a large inductor is required for the tunable IMN. Through the above approach, $L_{\max}$ is effectively decreased from 1400 nH to 750 nH. It also helps to avoid the expansion of tuning range of C_{n_t} and system performance degradation.

C. Dynamic Tuning System

The input impedance of the transmitting coil $Z_{\text{in\_}c}$ can be obtained by measuring the input voltage and output voltage of the IMN, V_{in} and V_{out}, as shown in Fig. 8. The input impedance $Z_{\text{in\_}c}$ is then calculated from the values of L_{n_t} and C_{n_t} of the IMN and the two voltages V_{in} and V_{out}, as expressed below [34]

$$Z_{\text{in\_}c} = \frac{1}{\left(\frac{V_{\text{in}}}{V_{\text{out}}} - 1\right) \cdot \frac{1}{j\omega L_{n\_t}} - j\omega C_{n\_t}}. \tag{7}$$

As shown in Fig. 8, the magnitude and phase of $V_{\text{in}}/V_{\text{out}}$ are measured by employing two log amplifiers, a voltage comparator, and a phase detector. In the following experiments, a dedicated chip, AD8302 from Analog Devices, is used for the above measurement. Based on the measured V_{in} and V_{out}, the

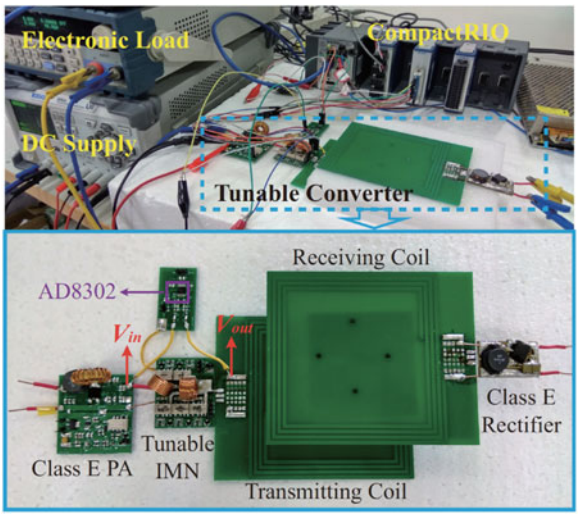

Fig. 9. Configuration of the dynamically controlled tunable converter.

TABLE II
CIRCUIT PARAMETERS OF THE TUNABLE IMN

L_{n1}	L_{n2}	C_{n1}	C_{n2}	C_{n3}
400 nH	600 nH	300 pF	450 pF	600 pF

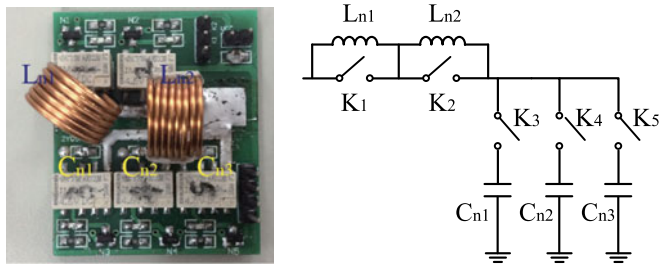

Fig. 10. Fabricated tunable IMN and its topology. (a) Circuit. (b) Topology.

load of the IMN (i.e., $Z_{\text{in\_}c}$) is calculated using (7). The desired L_{n_t}, C_{n_t}, and C_s are then determined to achieve high efficiency and stable output power through a look-up table or other more sophisticated tuning algorithms [31]. The purpose of this paper is to analyze, implement, and validate the tunable Class E^2 DC–DC converter for WPT applications. Thus, a straightforward solution, the look-up table, is used to determine the above three parameters under different measured $Z_{\text{in\_}c}$.

IV. EXPERIMENTAL VALIDATION

Three Class E^2 DC–DC converters for 6.78 MHz WPT, i.e., conventional converter, converter with fixed IMN, and tunable converter, are fabricated and compared. The circuit parameters shown in Table I are applied in the conventional converter. The SUD06N10 (MOSFET) and STPSC406D (Diode) are used as switches in the PA and rectifier, respectively. The coupling coefficient k varies from 0.1 to 0.4 by changing the distance between the coupling coils from 1 to 5.2 cm. The DC load of the rectifier is emulated by an electronic load. The DC supply voltage is kept constant, 20 V, in all experiments. The other two converters are realized by adding the fixed and tunable IMN into the conventional converter, respectively. L_n and C_n used in the fixed IMN are 690 nH and 570 pF, respectively.

Fig. 9 shows the fabricated tunable converter. Note that C_{tx} should be changed to 175 pF in the tunable converter. Relay switches are utilized to realize the tunable inductor and capacitor. The required peak current and voltage for the inductors (2 A and 54 V) and capacitors (1.6 A and 110 V) are obtained through simulation. Murata GCM series capacitors with 100 Vdc rated voltage are employed. The inductors are fabricated in house using 0.75-mm copper wire. The parameters of the tunable IMN are listed in Table II. The gain and phase detector, AD8302, is used to measure the magnitude and phase of $V_{\text{in}}/V_{\text{out}}$. V_{in} and V_{out} are the input voltage and output voltage of the tunable IMN. From the data sheet, the power consumption of AD8302 is about 0.1 W, which is neglectable in the following experiments. The tuning algorithm is then implemented over National Instruments CompactRIO system. Here a look-up table is applied to determine the desired values of L_{n_t}, C_{n_t}, and C_s, and thus the control signals for the switches. Table III shows an example look-up table used in the following experiments. The binary data represent the combinations of states of the switches, K_1–K_6. "1" and "0" correspond to ON and OFF states, respectively. Here, K_1–K_5 are the switches shown in Fig. 10(b) and K_6 is the switch to tune C_s in PA. Note that C_s is 215 pF when K_6 is 0 and 420 pF when K_6 is 1.

As discussed in Section II, the deterioration of system performance under the varying operation condition is mostly due to the mismatch of the PA load. Fig. 11 shows the drain voltage V_{DS} of the Class E PA in the these three converters. V_{DS} in the conventional converter is very high at the end of OFF state when the operation condition deviates from the optimum one, as illustrated in Fig. 11(d), (g), and (j). These results indicate that the PA is in a hard-switching operation, and thus with high switching loss. Meanwhile, in the most cases V_{DS} in the converters with fixed and tunable IMNs approaches zero before the ON state. This shows that the load mismatch of PA is largely improved by having the IMNs, namely the soft-switching operation of the PA. The Class E PA is driven with 50% duty cycle. But duty cycle smaller than 50% and sudden change of the duty cycle are observed such as in Fig. 11(h) and (k). They are caused by the mismatched PA load, which may lead to a negative drain voltage. Due to the parasitic diode in the N-channel MOSFET, the actual drain voltage becomes zero when the negative drain voltage is about to occur. This explains a smaller duty cycle than 50%.

The system efficiency η_{sys} and output power P_{load} of the conventional Class E^2 DC–DC converter, converter with fixed IMN, and tunable converter are shown and compared in Fig. 12. The efficiency of the conventional Class E^2 DC–DC converter drops significantly when k and R_{load} change. The lowest efficiency is 20%. At the same time, the efficiencies of the converter with fixed IMN and the tunable converter keep high over 62% even when the coupling coefficient k and DC load R_{load} vary in a wide range. In terms of efficiency, the tunable converter

TABLE III
LOOK-UP TABLE IN EXPERIMENTS

R_{load} (Ω) / k	10	20	30	40	50	60	70	80	90	100
0.1	110000	111000	111100	110110	110110	111110	111110	111110	111110	111110
0.2	010100	011000	010100	010010	010010	011100	011010	011010	010110	010110
0.3	100101	100011	100011	101101	101101	101101	101011	101011	101011	101011
0.4	001001	000101	000101	000101	000101	000011	000011	000011	000011	000011

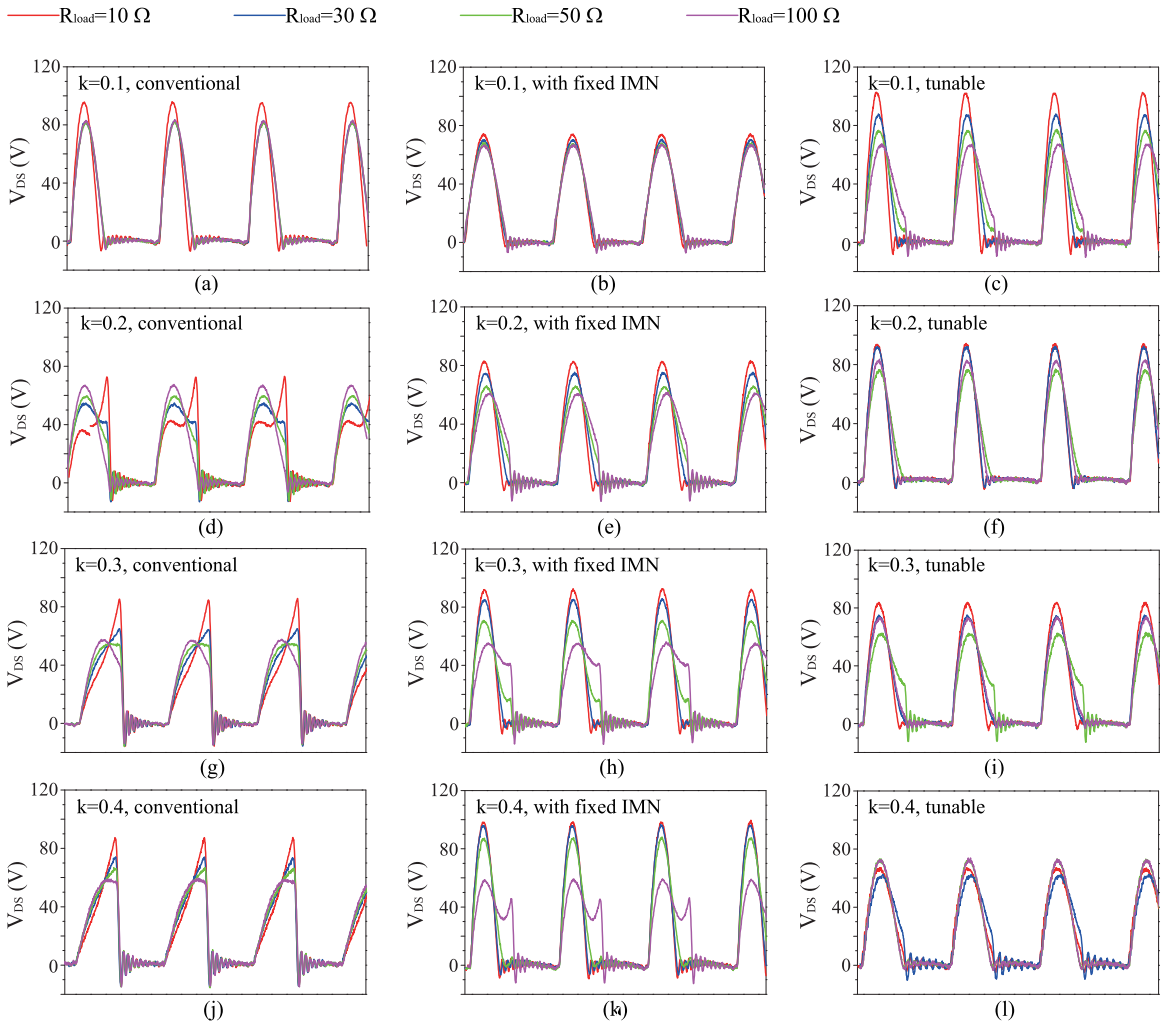

Fig. 11. Drain voltage V_{DS} of PA for the conventional converter, converter with fixed IMN, and tunable converter under different k and R_{load}. (a)–(c) $k = 0.1$. (d)–(f) $k = 0.2$. (g)–(i) $k = 0.3$. (j)–(l) $k = 0.4$.

does not show an obvious advantage over the converter using the fixed IMN. But it provides stable output power about 9 W. Note that the actual output power may reach to 5.6 W in certain cases such as in Fig. 12(b). This deviation from the target output power is mainly caused by the quantization error due to the combination of discrete inductors and capacitors. The error could be mitigated by adding more components (i.e., inductors, capacitors, and switches) in the tunable IMN or introducing continuously tunable components. At the same time, there is always a tradeoff between improved matching performance and increased complexity and cost. Compared with the tunable converter, the output power of the conventional converter and converter with the fixed IMN varies substantially when k and R_{load} change. P_{load} varies from 2 to 15.2 W in the conventional converter and 0.96 to 20.4 W in the converter with the fixed IMN. This large variation in the output power is undesirable in real applications. The above experiments validate the feasibility of the proposed tunable converter. High system efficiency and stable output power are simultaneously achieved through the tunable IMN and with reduced tuning range. The tunable converter makes the 6.78-MHz WPT system robust against variations in real operation conditions.

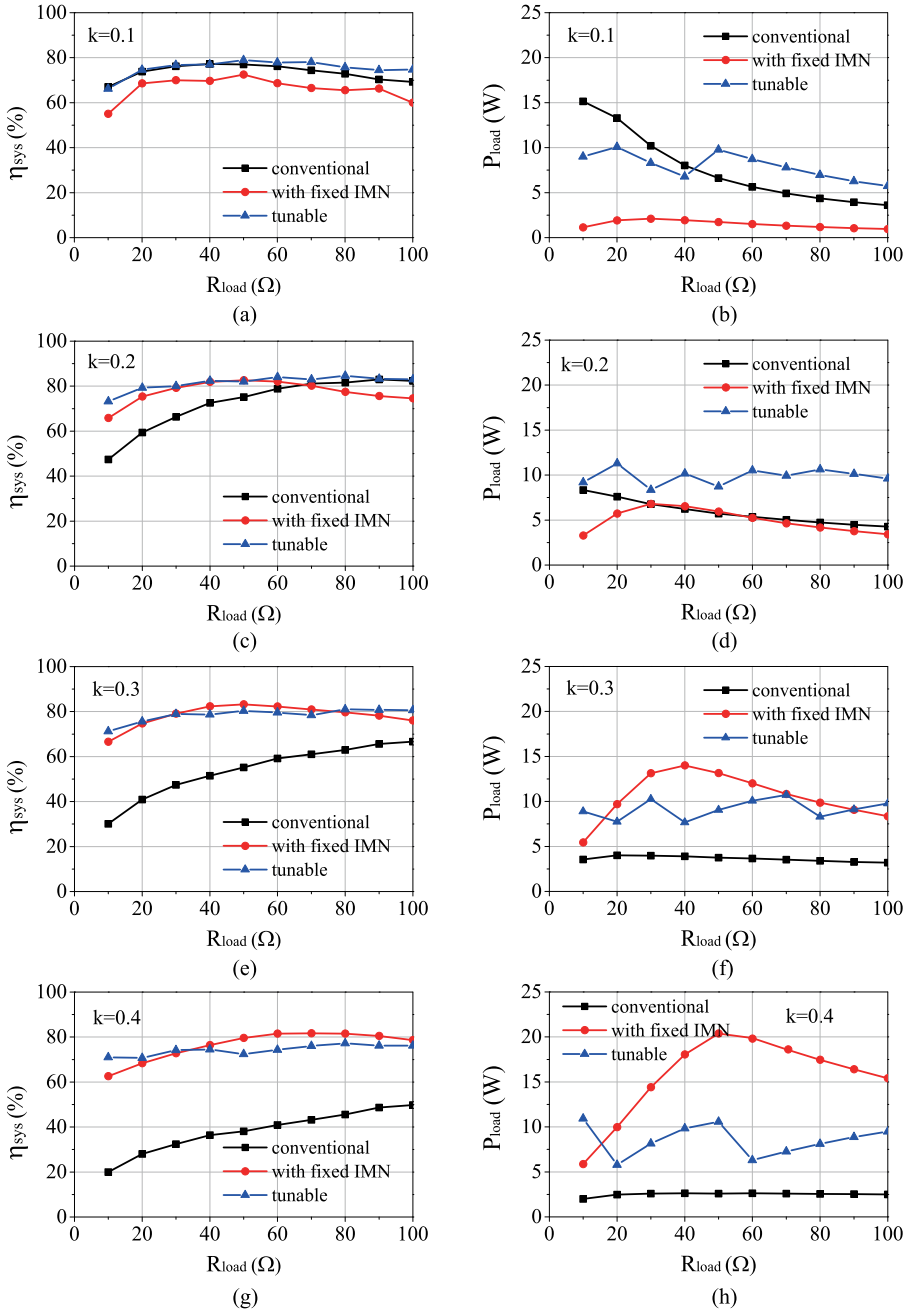

Fig. 12. Efficiencies and output power of the conventional Class E^2 DC–DC converter, converter with fixed IMN, and tunable converter when k and $R_{\rm load}$ change. (a) and (b) $k = 0.1$. (c) and (d) $k = 0.2$. (e) and (f) $k = 0.3$. (g) and (h) $k = 0.4$.

V. Conclusion

Class E^2 DC–DC converter is attractive for WPT applications due to its high system efficiency. But the converter is also sensitive to the variations in operation condition. Its system efficiency may dramatically drop when the DC load and coupling coefficient deviate from their optimum values. The deterioration of system performance is mainly caused by the mismatch of PA load, which can be improved by introducing an L-type IMN. In this paper, a high-efficiency region in the Smith chart is first defined. A fixed IMN is shown to be sufficient to achieve high efficiency by transforming PA load to the high-efficiency region. In order to also obtain stable output power under large variations in coil coupling and DC load, a tunable IMN is proposed and designed. The high system efficiency is ensured by proper selection of IMN topology (L-type) and parameter optimization. The required tuning range of the tunable IMN is further reduced by modifying the parameters of the coupling coils and PA. The conventional Class E^2 DC–DC converter, converter with fixed IMN, and proposed tunable converter are fabricated and compared in experiments. The results show that high efficiency and stable output power are simultaneously achieved by the tunable converter with reduced tuning range, and thus validate the proposed solution.

REFERENCES

[1] M. Liu, M. Fu, and C. Ma, "Low-harmonic-contents and high-efficiency Class E full-wave current-driven rectifier for megahertz wireless power transfer systems," *IEEE Trans. Power Electron.*, vol. 32, no. 2, pp. 1198–1209, Feb. 2017.

[2] J. Choi, D. Tsukiyama, Y. Tsuruda, and J. M. Rivas, "High-frequency, high-power resonant inverter with eGaN FET for wireless power transfer," *IEEE Trans. Power Electron.*, to be published. doi:10.1109/TPEL.2017.2740293.

[3] N. O. Sokal and A. D. Sokal, "Class E–A new class of high-efficiency tuned single-ended switching power amplifiers," *IEEE J. Solid-State Circuits*, vol. 10, no. 3, pp. 168–176, Jun. 1975.

[4] P. Srimuang, N. Puangngernmak, and S. Chalermwisutkul, "13.56 MHz Class E power amplifier with 94.6% efficiency and 31 watts output power for RF heating applications," in *Proc. IEEE Elect. Eng./Electron., Comput., Telecommun. Inf. Technol.* Nakhon Ratchasima, Thailand: IEEE, May 2014, pp. 1–5.

[5] S. Liu, M. Liu, S. Yang, C. Ma, and X. Zhu, "A novel design methodology for high-efficiency current-mode and voltage-mode Class-E power amplifiers in wireless power transfer systems," *IEEE Trans. Power Electron.*, vol. 32, no. 6, pp. 4514–4523, May 2017.

[6] S. Aldhaher, P. C.-K. Luk, K. E. K. Drissi, and J. F. Whidborne, "High-input-voltage high-frequency Class E rectifiers for resonant inductive links," *IEEE Trans. Power Electron.*, vol. 30, no. 3, pp. 1328–1335, Mar. 2015.

[7] P. C.-K. Luk, S. Aldhaher, W. Fei, and J. F. Whidborne, "State-space modeling of a Class E^2 converter for inductive links," *IEEE Trans. Power Electron.*, vol. 30, no. 6, pp. 3242–3251, Jun. 2015.

[8] T. Nagashima, K. Inoue, X. Wei, E. Bou, E. Alarcón, and H. Sekiya, "Inductively coupled wireless power transfer with Class-E^2 DC-DC converter," in *Proc. Eur. Conf. Circuit Theory Des*. Dresden, Germany: IEEE, Sep. 2013, pp. 1–4.

[9] M. Liu, M. Fu, and C. Ma, "Parameter design for a 6.78-MHz wireless power transfer system based on analytical derivation of Class E current-driven rectifier," *IEEE Trans. Power Electron.*, vol. 31, no. 6, pp. 4280–4291, Jun. 2016.

[10] T. C. Beh, M. Kato, T. Imura, S. Oh, and Y. Hori, "Automated impedance matching system for robust wireless power transfer via magnetic resonance coupling," *IEEE Trans. Ind. Electron.*, vol. 60, no. 9, pp. 3689–3698, Sep. 2013.

[11] B. H. Waters, A. P. Sample, and J. R. Smith, "Adaptive impedance matching for magnetically coupled resonators," in *Proc. Progress Electromagn. Res. Symp.*, Moscow, Russia, Aug. 2012, pp. 694–701.

[12] M. Liu, Y. Qiao, S. Liu, and C. Ma, "Analysis and design of a robust Class E^2 DC-DC converter for megahertz wireless power transfer," *IEEE Trans. Power Electron.*, vol. 32, no. 4, pp. 2835–2845, Apr. 2017.

[13] S. Aldhaher, P. C.-K. Luk, A. Bati, and J. F. Whidborne, "Wireless power transfer using Class E inverter with saturable DC-feed inductor," *IEEE Trans. Ind. Appl.*, vol. 50, no. 4, pp. 2710–2718, Jul. 2014.

[14] S. Aldhaher, P. C.-K. Luk, and J. F. Whidborne, "Electronic tuning of misaligned coils in wireless power transfer systems," *IEEE Trans. Power Electron.*, vol. 29, no. 11, pp. 5975–5982, Nov. 2014.

[15] S. Aldhaher, C. K. Luk, and J. F. Whidborne, "Tuning Class E inverters applied in inductive links using saturable reactors," *IEEE Trans. Power Electron.*, vol. 29, no. 6, pp. 2969–2978, Jun. 2014.

[16] Y. F. Li and C. S. Tseng, "Tracking control of Class E inverter for the duty cycle control," in *Proc. Int. Symp. Ind. Electron*. Istanbul, Turkey: IEEE, Jun. 2014, pp. 2643–2647.

[17] A. P. Sample, B. H. Waters, S. T. Wisdom, and J. R. Smith, "Enabling seamless wireless power delivery in dynamic environments," *Proc. IEEE*, vol. 101, no. 6, pp. 1343–1358, Jun. 2013.

[18] A. Trigui, S. Hached, F. Mounaim, A. C. Ammari, and M. Sawan, "Inductive power transfer system with self-calibrated primary resonant frequency," *IEEE Trans. Power Electron.*, vol. 30, no. 11, pp. 6078–6087, Nov. 2015.

[19] A. P. Sample, D. T. Meyer, and J. R. Smith, "Analysis, experimental results, and range adaptation of magnetically coupled resonators for wireless power transfer," *IEEE Trans. Ind. Electron.*, vol. 58, no. 2, pp. 544–554, Feb. 2011.

[20] B. Wang, K. H. Teo, T. Nishino, W. Yerazunis, J. Barnwell, and J. Zhang, "Experiments on wireless power transfer with metamaterials," *Appl. Phys. Lett.*, vol. 98, no. 25, Jun. 2011, Art. no. 254101.

[21] J. P. K. Sampath, A. Alphones, and D. M. Vilathgamuwa, "Figure of merit for the optimization of wireless power transfer system against misalignment tolerance," *IEEE Trans. Power Electron.*, vol. 32, no. 6, pp. 4359–4369, Jun. 2017.

[22] W. Zhong and S. Y. R. Hui, "Reconfigurable wireless power transfer systems with high energy efficiency over wide load range," *IEEE Trans. Power Electron.*, to be published. doi: 10.1109/TPEL.2017.2748161.

[23] J. Lee, K. Lee, and D. H. Cho, "Stability improvement of transmission efficiency based on relay resonator in wireless power transfer system," *IEEE Trans. Power Electron.*, vol. 32, no. 5, pp. 3297–3300, May 2017.

[24] W. Zhong and S. Hui, "Maximum energy efficiency tracking for wireless power transfer systems," *IEEE Trans. Power Electron.*, vol. 30, no. 7, pp. 4025–4034, Jul. 2015.

[25] M. Fu, C. Ma, and X. Zhu, "A cascaded boost–buck converter for high-efficiency wireless power transfer systems," *IEEE Trans. Ind. Informat.*, vol. 10, no. 3, pp. 1972–1980, Aug. 2014.

[26] M. Fu, H. Yin, X. Zhu, and C. Ma, "Analysis and tracking of optimal load in wireless power transfer systems," *IEEE Trans. Power Electron.*, vol. 30, no. 7, pp. 3952–3963, Jul. 2015.

[27] J. A. Santiago-González, K. M. Elbaggari, K. K. Afridi, and D. J. Perreault, "Design of Class E resonant rectifiers and diode evaluation for VHF power conversion," *IEEE Trans. Power Electron.*, vol. 30, no. 9, pp. 4960–4972, Sep. 2015.

[28] L. Roslaniec, A. S. Jurkov, A. Al Bastami, and D. J. Perreault, "Design of single-switch inverters for variable resistance/load modulation operation," *IEEE Trans. Power Electron.*, vol. 30, no. 6, pp. 3200–3214, Jun. 2015.

[29] D. M. Pozar, *Microwave Engineering*. Hoboken, NJ, USA: Wiley, 2009.

[30] M. Thompson and J. K. Fidler, "Determination of the impedance matching domain of impedance matching networks," *IEEE Trans. Circuits Syst. I, Reg. Papers*, vol. 51, no. 10, pp. 2098–2106, Oct. 2004.

[31] Q. Gu, J. R. De Luis, A. S. Morris, and J. Hilbert, "An analytical algorithm for pi-network impedance tuners," *IEEE Trans. Circuits Syst. I*, vol. 58, no. 12, pp. 2894–2905, Dec. 2011.

[32] P. Sjoblom and H. Sjoland, "An adaptive impedance tuning CMOS circuit for ISM 2.4-GHz band," *IEEE Trans. Circuits Syst. I, Reg. Papers*, vol. 52, no. 6, pp. 1115–1124, Jun. 2005.

[33] R. Rhea, "The Yin-Yang of matching: Part 1—Basic matching concepts," *High Freq. Electron.*, vol. 5, no. 3, pp. 16–25, Jun. 2006.

[34] Q. Gu and A. S. Morris, "A new method for matching network adaptive control," *IEEE Trans. Microw. Theory Tech.*, vol. 61, no. 1, pp. 587–595, Jan. 2013.

Shuangke Liu (S'15) received the B.S. degree in electronics and information engineering from Xidian University, Xian, China, in 2013. She is currently working toward the Ph.D. degree in electrical and computer engineering at University of Michigan–Shanghai Jiao Tong University Joint Institute, Shanghai Jiao Tong University, Shanghai, China.

Her research interests include optimal design of high-frequency wireless power transfer systems and RF/microwave circuit design.

Ming Liu (S'15–M'17) received the B.S. degree from SiChuan University, Sichuan, China, in 2007, and the M.S. degree from the University of Science and Technology Beijing, Beijing, China, in 2011, both in mechatronics engineering, and the Ph.D. degree in electrical and computer engineering from the University of Michigan–Shanghai Jiao Tong University Joint Institute, Shanghai Jiao Tong University, Shanghai, China, in 2017.

He is currently a Postdoctoral Research Fellow in the Department of Electrical Engineering, Princeton University, Princeton, NJ, USA. Between 2012 and 2014, he was an Assistant Research Fellow with the Shenyang Institute of Automation, Chinese Academy of Sciences, Shenyang, China. His research interests include high-frequency resonant converters, wireless power transfer systems, power electronics and applications, and circuit-level and system-level optimization.

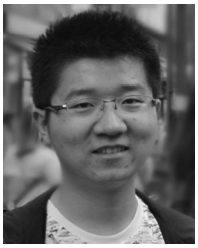

Songyang Han (S'17) received the B.E. degree in automation from Nanjing University, Nanjing, China, in 2015. He is currently working toward the M.S. degree in electrical and computer engineering at the University of Michigan–Shanghai Jiao Tong University Joint Institute, Shanghai Jiao Tong University, Shanghai, China.

His research interests include embedded control and hardware, energy management of microgrids, game theory, and data mining.

Xinen Zhu (S'04–M'09) received the B.Eng. (Hons.) degree in electronic and communication engineering from City University of Hong Kong, Hong Kong, in 2003, and the M.S. and Ph.D. degrees both in electrical engineering from the University of Michigan at Ann Arbor, Ann Arbor, MI, USA, in 2005 and 2009, respectively.

He was an Assistant Professor of electrical and computer engineering with the University of Michigan–Shanghai Jiao Tong University Joint Institute, Shanghai Jiao Tong University, Shanghai, China, from 2009 to 2017. He is currently an R&D Director of RF Technology, the Shanghai Industrial μ Technology Research Institute, Shanghai, China. His research interests include ferroelectric thin films, RF/microwave circuits, wireless power transfer, and millimeter wave radar.

Chengbin Ma (M'05) received the B.S. (Hons.) degree in industrial automation from the East China University of Science and Technology, Shanghai, China, in 1997, and the M.S. and Ph.D. degrees both in electrical engineering from the University of Tokyo, Tokyo, Japan, in 2001 and 2004, respectively.

He is currently an Associate Professor of electrical and computer engineering at the University of Michigan–Shanghai Jiao Tong University Joint Institute, Shanghai Jiao Tong University, Shanghai, China. Between 2006 and 2008, he held a Postdoctoral position with the Department of Mechanical and Aeronautical Engineering, University of California Davis, CA, USA. From 2004 to 2006, he was an R&D Researcher with Servo Laboratory, Fanuc Limited, Yamanashi, Japan. His research interests include energy management, megahertz wireless power transfer, dynamics and motion control, and wide applications in electronic devices, electric vehicles, networked multiphysics systems such as microgrids and smart grids, etc.

Dr. Ma is an Associate Editor of the IEEE TRANSACTIONS ON INDUSTRIAL INFORMATICS and the IEEE INDUSTRIAL ELECTRONICS Technical News.